Noisy and regular features in Saffman-Taylor patterns

M. W. DiFrancesco and J. V. Maher
Department of Physics and Astronomy, University of Pittsburgh, Pittsburgh, Pennsylvania 15260
(Received 20 May 1988; revised manuscript received 5 December 1988)

Fourteen realizations of Saffman-Taylor flow at small-viscosity contrast have been measured under nearly identical flow conditions. With control-parameter fluctuations $\lesssim 0.15\%$, we observe fluctuations of 20% in the crudest measures of the patterns and much larger fluctuations in the strengths of individual wave numbers of a modal analysis of the patterns for this broadband instability. The initial disturbance can be observed as it propagates toward the center of the cell from the side walls. As the patterns go over from the linear to the nonlinear regime, several quantitative measures show abrupt change. In the nonlinear regime the patterns not only fail to show progress toward a single-finger steady state but the individual fingers actually show a tendency to evolve toward a narrower distribution of lengths.

I. INTRODUCTION

Saffman-Taylor fingering represents the simplest of pattern formation problems,[1-3] yet its only currently understood feature is its fully developed single-finger steady-state pattern.[1,4-6] While the earliest stages of the development of the fingering pattern are at least qualitatively predicted by linear-stability theory, the patterns rapidly develop into a complex nonlinear regime for which the few available calculations[7,8] have not given close agreement with observations.[9,10] While these patterns are widely assumed to go over eventually to the single-finger steady state, under some conditions it is not possible to observe the pattern long enough to see any progress in this direction. In fact, only in cells which are not much wider than λ, the wavelength of the fastest-growing mode from the linear-stability analysis, is it generally possible to observe the pattern long enough to see the steady-state solution.

Of the two control parameters for viscous fingering flow, only one, the dimensionless interfacial tension B, scales out of the dimensionless Hele-Shaw equations.[7] The other, the dimensionless viscosity contrast A, appears explicitly in the equations; therefore, even though a single-finger steady state should still exist and linear-stability analysis predicts patterns which can be mapped onto each other for all A, the early and late mappings are different and the dynamical path between early and steady-state patterns could be A dependent in a nontrivial way. With one exception,[9] previous work on Saffman-Taylor flow has concentrated on large values of A.

We have performed an extensive set of measurements on this instability at very small values of A in the linear and early nonlinear regime, using a critical binary-liquid mixture to allow convenient and precise determination of the control parameters (as will be discussed in detail below.) In this paper we report on our study of the fluctuations in the viscous fingering patterns we observed and on the regular and highly reproducible features of the flow. Just as computer simulations can frequently show noisy behavior in parameters which one might originally have expected to be stable, it is important in experimental nonlinear physics to check carefully to see which experimental observations are easily reproducible and which involve strong fluctuations. Beyond mere checking for reproducibility, it is interesting to quantify which features of a nonlinear system are stable and contribute to the recognizeable pattern and which provide the variations. We have measured a small ensemble of 14 realizations of a Saffmann-Taylor flow under "identical" flow conditions and have subjected the observed patterns to extensive statistical analysis. Section II contains a very brief description of the experiment. In Sec. III the data are presented and their most obvious regularities discussed. Then, in Sec. IV we discuss several attempts at using statistical and modal analyses to produce a quantitative characterization of the patterns and their fluctuations.

II. THE EXPERIMENT

The Saffman-Taylor instability[1] arises at the initially planar interface between two fluids flowing in a Hele-Shaw cell (a cell formed by parallel plates with a gap between them of thickness b where b is smaller than any other length scale in the problem). It is driven either by a pressure gradient advancing the less viscous fluid against the more viscous, or by gravity as a result of a density difference between the fluids. For the case of gravity-driven flow in a closed rectangular cell where the average velocity of the interface is zero, the dispersion relation, from linear stability analysis,[1,2] takes the form

$$i\omega(2\bar{\mu}/K)-(\rho_2-\rho_1)gk+\sigma^* k^3=0 , \quad (1)$$

where $K\equiv b^2/12$ is a mobility. The average shear viscosity, the effective interfacial surface tension, the density of fluid n, and the acceleration due to gravity are represented by $\bar{\mu}$, σ^*, ρ_n, and g, respectively. This dispersion relation predicts broadband instability for all wave numbers k below a critical value

$$k_c=[(\rho_2-\rho_1)g/\sigma^*]^{1/2} . \quad (2)$$

Tryggvason and Aref (TA) (Ref. 7) have shown that the problem can be recast in terms of two dimensionless control parameters A and B, where A is a dimensionless viscosity contrast

$$A=\frac{\mu_2-\mu_1}{\mu_2+\mu_1} , \quad (3)$$

B is a dimensionless surface tension (or inverse capillary number)

$$B=\sigma^* b^2/[6U^* W^2(\mu_2+\mu_1)] , \quad (4)$$

with W the width of the Hele-Shaw cell, and U^* a characteristic velocity

$$U^*=\frac{(\rho_1-\rho_2)gb^2}{12(\mu_1+\mu_2)} . \quad (5)$$

TA show that B can be scaled out of the two-dimensional Hele-Shaw equations by adopting the dimensionless time

$$t'=U^* t/1.84WB^{1/2} \quad (6)$$

and the dimensionless length

$$x'=x/7.70WB^{1/2} . \quad (7)$$

We have added the factors 1.84 and 7.70 in Eqs. (6) and (7) to make the fastest growing wavelength (in the linear stability analysis) and its growth rate both equal 1. As was mentioned above, the viscosity contrast A cannot be scaled out of the equations. Wall effects are known[3] to modify the Hele-Shaw equations, and we will not discuss attempts at empirical scaling in this paper. The present paper focuses on fluctuations observed at one definite combination of A and B.

The central experimental feature of this work is to exploit the well-known features of critical binary liquids to vary the control parameters of the Saffman-Taylor flow. This eliminates the need to change liquids when varying the control parameters and also provides enormous precision in the knowledge of values of and changes in the control parameters. We used a critical mixture of isobutyric acid and water (IBW) which has its nominal critical temperature[11] T_c, at 26.12 °C. The exact value of T_c for a given sample is known to depend quite sensitively on the exact composition of the isobutyric-acid source, but the critical properties of the system are not affected. Our typical sample showed $T_c=26.21$ °C. Our samples were made up to phase separate never more than 10^{-5} °C below T_c, and we remeasured T_c before each of the several major sets of measurements to be presented below.

Our Hele-Shaw cell consisted of a commercially available $45\times45\times1$ mm^3 spectrophotometric cell.[12] The cell gap $b=1$ mm is smaller than, but not much smaller than the ~5-mm wavelength observed in the patterns to be discussed below. Other than for wetting corrections to the two-dimensional equations,[3] it is difficult to estimate the length-scale ratio at which three-dimensional effects should become important, but a previous study[9] suggests that a 5-to-1 ratio produces results which are similar to flows at much larger ratio and that observable three-dimensional effects set in very gently near a ratio of 3 to 1. The sealed cell was immersed in a temperature-controlled water bath, and temperature fluctuations were restricted to be less than 0.3 mK over periods of hours and 1 mK over days. This temperature control allows one confidence in calculating the viscosity and density contrasts and the interfacial tension between the two liquid phases. Unstable flows were realized by setting the temperature of the system at the desired value in the two-phase region of the liquid mixture's phase diagram, mixing the liquids to achieve equilibrium composition, allowing the system time to form a stable, flat meniscus, and then inverting the cell to put the denser, higher-viscosity fluid on top. The flow was measured by a 35-mm camera whose motor drive was set to advance film frames at a rate appropriate to the speed of the flow. We were always able to measure at least several frames in the linear regime (interface oscillation amplitude less than wavelength) with a typical camera rate of 2 frames/sec.

The data measured in the earliest version of this experiment were quite tedious to analyze because the interface between the two fluid phases is not easy to see and becomes progressively more difficult to see as the critical temperature is approached (and the physical difference between the two phases vanishes). We have circumvented this difficulty by learning to dye the isobutyric-acid–rich phase with a sensitive red pH marker.[13] The addition of such an impurity would be expected to shift T_c but not to change the critical properties of the liquid mixture in any important way, but to be certain of this we performed a series of duplicate measurements, comparing the Saffman-Taylor flows between dyed and undyed samples, and found no significant differences in the averages and standard deviations of the stable features of the flow. Most of the data presented below were measured on a dyed sample.

The photographs of the developing interface were digitized with a GTCo digitizing tablet[14] and processed by computer. The digitized interface represents a one-dimensional object (a long stream of addresses, each of which is specified by two numbers). As such, it lends itself to retaining very great spatial resolution, far greater than would be convenient with a two-dimensional array of pixels. During digitization the magnified images of the photographic slides could be measured to a precision limited only by the experimenter's hand jitter (typically 0.5 mm). With this precision it has been possible to be confident in extracting the spatial measures discussed below, including the curvature which involves a second derivative of the spatial distribution. (For further discussion of spatial resolution, see Ref. 15.)

When the temperature of the IBW sample is changed, both control parameters A and B are changed. The contrast in shear viscosities for the binary-liquid mixture is proportional to the contrast in mass densities $\rho_2-\rho_1$, since the kinematic viscosities of the two liquid phases are equal to a very good approximation. The mass-density contrast is known to vary as ϵ^β, where $\epsilon=(T_c-T)/T_c$ and $\beta=0.33$. Similarly, interfacial ten-

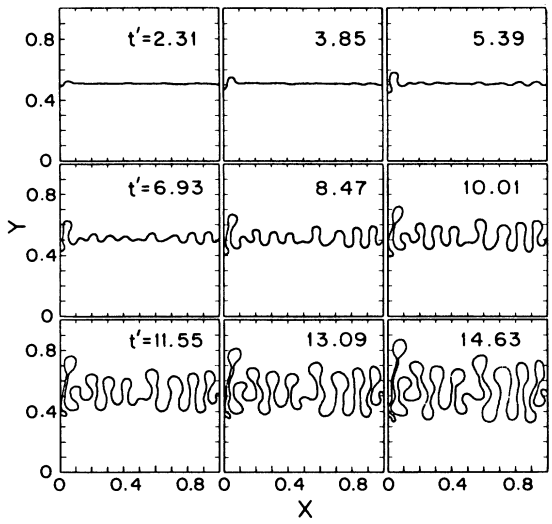

FIG. 1. Fingering pattern development for one flow in the ensemble. Dimensionless time t' is indicated for each frame. Positions x and y are in units of cell width $W=4.5$ cm.

sion is known to vary as ϵ^{μ}, where $\mu=1.25$. These properties give $A=0.027\epsilon^{\beta}$ and $B=0.022\epsilon^{\mu-\beta}$. The uncertainty in A is presumably very small. The critical coefficient for the mass-density contrast has an uncertainty of about 2%. Further contributions to the uncertainty arise merely from the very small temperature fluctuations discussed above and from the uncertainty in the assumption that the kinematic viscosities of the two fluid phases are identical. These latter effects give a relative uncertainty in A of $\lesssim 0.03\%$. The uncertainty in the absolute value of B is estimated to be 25%, because of the uncertainty in the critical coefficient of the interfacial tension. However, the reproducibility of B on our laboratory apparatus is limited only by our temperature control and our ability to align the cell with the vertical, and so the fluctuations in our B are $\Delta B/B \approx 0.15\%$.

Using the temperature control just described, we have studied flows with characteristic finger widths from $\frac{1}{5}$ to $\frac{1}{15}$ the width of the cell, W. Most of these results will be presented in a future paper. Here, we limit our discussion to the "ensemble" measured at $A=5.56\times10^{-3}$, $B=2.13\times10^{-4}$, and we concentrate on the intrinsic fluctuations and their importance in comparison with average properties of the flow. Figure 1 shows the pattern development for one realization of the ensemble. Other realizations would look quite similar to the eye, just as an array of 14 snowflakes grown under similar conditions might look similar to the eye, while differing significantly in detail.

III. RESULTS OF MEASUREMENTS

To address the issue raised in the Introduction above concerning the role of noise in setting up the Saffman-Taylor flow and the identification of "noisy" observables in both early and later stages of the flow, we have selected the arbitrary point $A=5.56\times10^{-3}$, $B=2.13\times10^{-4}$ and

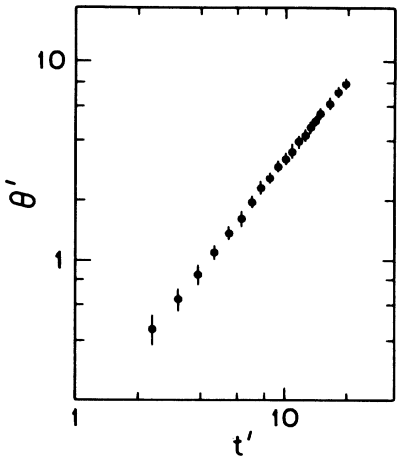

FIG. 2. Ensemble average of the dimensionless length of the mixing zone Θ' vs dimensionless time, as discussed in text.

then measured and extensively analyzed a small "ensemble" of data—14 flows whose flow conditions are as close to identical as our apparatus would allow. In this section we present these data in the various forms which will be useful for the discussion in later sections. Since several of the observable measures of the flow have not been defined above, it is also convenient to define them here. The error bars shown on the data presented in this section come from the standard deviations of the measurements in 14 realizations in the ensemble; the measurement errors from photographing and digitizing any one realization are so small that they do not contribute observably to the stated uncertainties.

Figure 2 shows the dimensionless length of the mixing zone Θ' versus dimensionless time for the ensemble of runs. Θ' is defined to be the length, along the direction of flow, of the region of the cell in which a cut across the width of the cell would find some of each phase of the fluid. Figure 3 shows the dimensionless stretching length

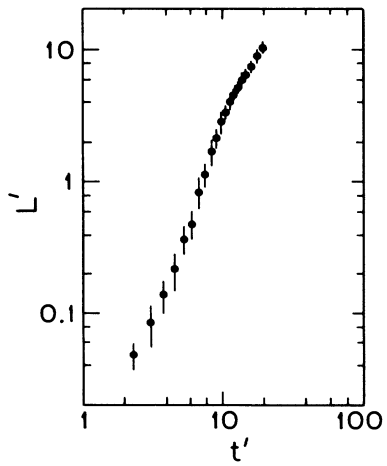

FIG. 3. Ensemble average of the dimensionless interface stretching length L' vs dimensionless time, as defined in the text.

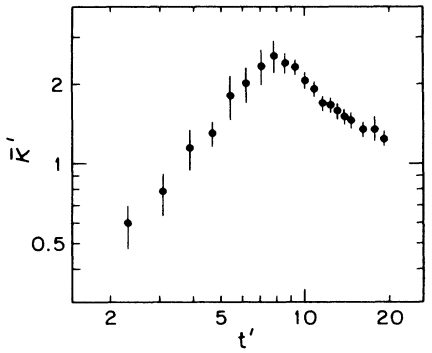

FIG. 4. Ensemble average of the average dimensionless interfacial curvature κ' vs dimensionless time.

L' of the interface versus dimensionless time. If the initial length of the interface is defined to be L_0 (in the present work L_0 is always identical to W, the width of the Hele-Shaw cell), and the integrated arc length of the interface at time t is $L(t)$, then $L'(t)=[L(t)-L_0]/L_0$. Figure 4 shows the dimensionless average curvature of the interface, $\bar{\kappa}'$ as a function of dimensionless time. By "curvature" we mean the absolute value of the curvature

$$\kappa=\frac{d\mathbf{T}}{ds} ,$$

where $\mathbf{T}$ is the unit tangent vector. We evaluated the curvature for the two-dimensional pattern; this does not account for the curvature across the narrow gap of thickness b but does capture the local detail of the two-dimensional pattern. For each measured interface, the average curvature is constructed as follows:

$$\bar{\kappa}=\int \kappa P(\kappa)d\kappa ,$$

where $P(\kappa)$ is the observed value of the normalized probability density of finding a point on the interface with curvature between κ and $\kappa+d\kappa$.

The obvious next step in attempting a quantitative analysis of the observed patterns would be to perform a model analysis. This approach is frustrated by the rapid ramification of the patterns which makes them multivalued functions of the position across the width of the cell at very early stages of the flow. In our earlier work[15] on radial Hele-Shaw flow, we addressed this problem by concentrating on curvature as a function of arc length and its Fourier transform. The two-dimensional curvature does indeed preserve all the local information about the two-dimensional pattern and so is, in principle, an acceptable choice for avoiding the multivaluedness of the direct pattern. This approach suffers, however, from an excess of detail; no information is lost and the intuition one might have about interpreting the complex details of the patterns themselves is less applicable to the power spectrum of the curvatures. For this reason, our earlier work was able to interpret only the first moment of the curvature power spectra. We have performed a curva-

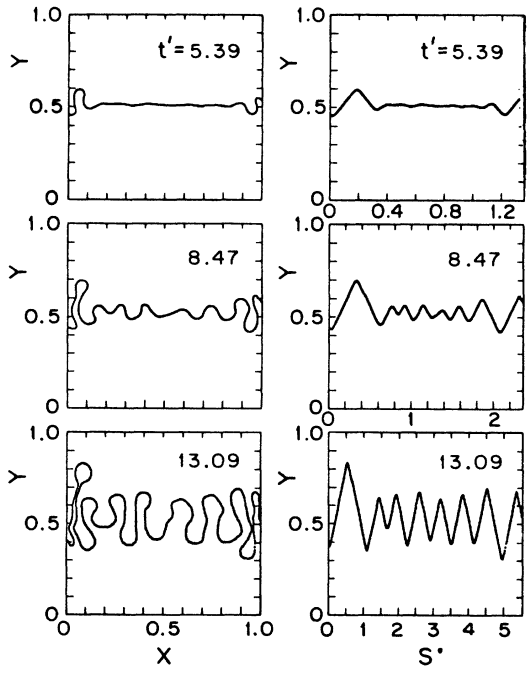

FIG. 5. On the left, patterns for one flow realization at the dimensionless times indicated. On the right, the y vs arc length s representations of the patterns on the left. Positions x, y, and s are in fractions of cell width.

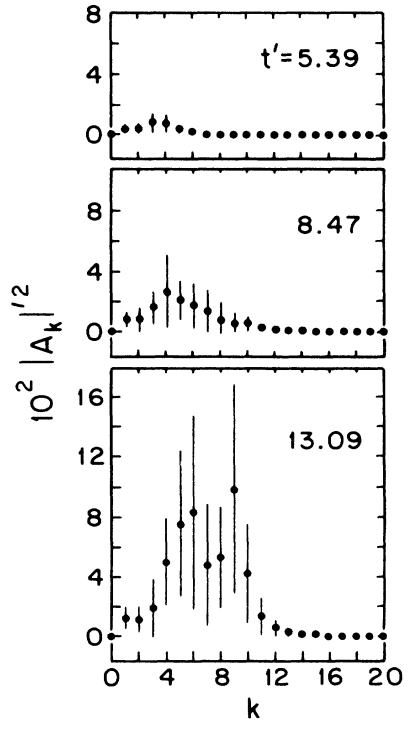

FIG. 6. Ensemble average of the squared dimensionless Fourier amplitude vs wave number of the y vs s representation of the patterns. Shown are the results for the same stages of development shown in Fig. 5. Wave numbers are in fractions of inverse total arc length.

ture analysis of our ensemble and have presented its first moment in Fig. 4 above, but for more extensive analysis we present an alternative approach which allows a meaningful model analysis to be applied to the ensemble while retaining much of the intuition one has about the individual patterns.

We generate single-valued functions which directly represent the spatial patterns by displaying the coordinates x and y versus the arc length s, where y is the interfacial position in the direction of flow and x is the position across the width of the cell. Figure 5 shows patterns from several stages of a flow realization on the left along with y versus s on the right. Long, thin fingers turn into sawtooth patterns in y, and when, at late times, the finger tips swell to look rather like balloons on the ends of strings; the effect is evident at the apexes of the sawtooth patterns. Figure 6 shows "power spectra" for y versus s at the same stages of development as are shown in Fig. 5. These power spectra are squared Fourier amplitudes versus wave number, and they result from averaging the individual power spectra for all 14 realizations in the ensemble. As always, the standard deviations shown in the figure arise from real fluctuations in the flow realizations with no significant effect from measurement uncertainties. Two effects are obvious: (1) the uncertainty is very large for any given wave number, and (2) the power spec-

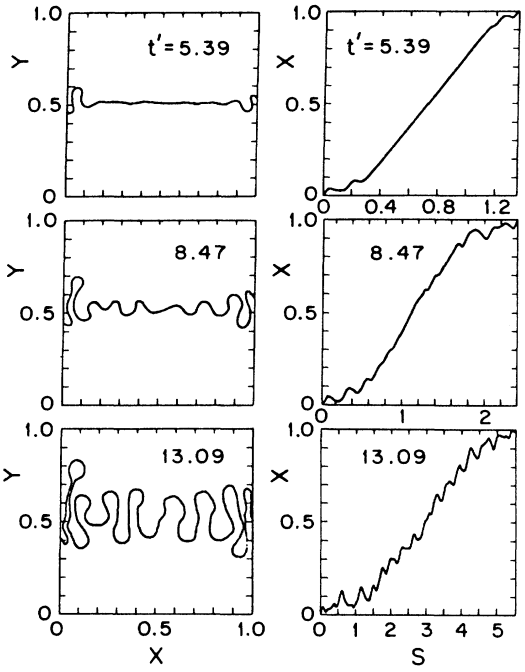

FIG. 8. The same patterns shown on the left of Fig. 5 paired with their corresponding x vs s representations. Positions x, y, and s are in fractions of cell width.

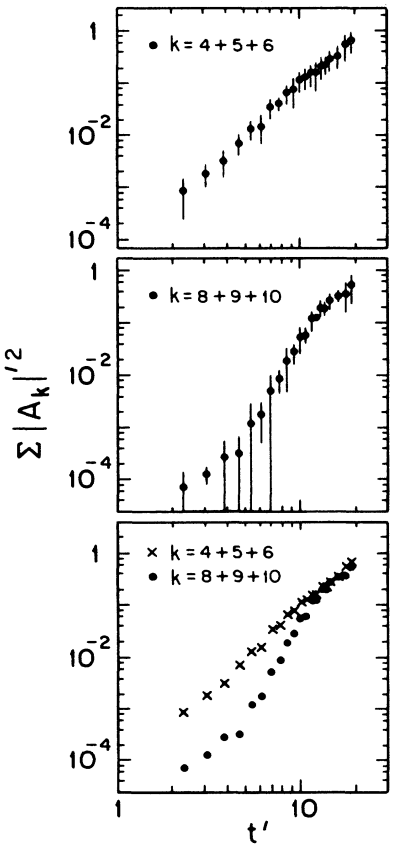

FIG. 7. Sums of the dimensionless power of neighboring wave numbers vs dimensionless time for the y vs s representation of flow patterns.

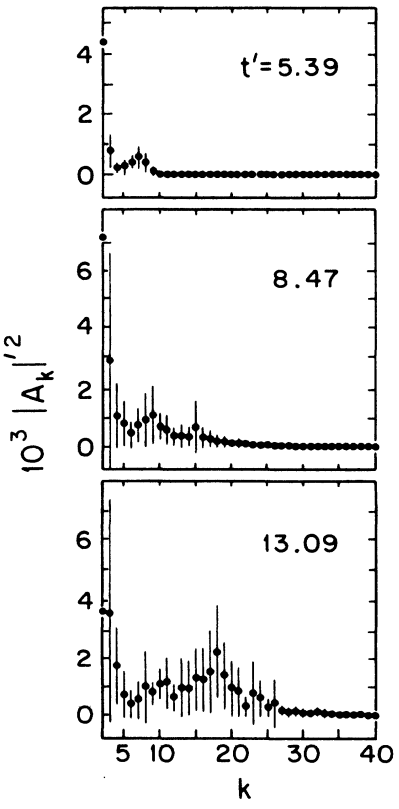

FIG. 9. Ensemble average of the squared dimensionless Fourier amplitude vs wave number of the x vs s representation of the patterns at the same development stages shown in Fig. 6. Wave numbers are in fractions of inverse total arc length.

trum is dominated at early times by low wave numbers and at later times by high wave numbers. The latter trend is further illustrated by Fig. 7, where sums of power in neighboring wave numbers are plotted versus time. The sum of $k=4$, 5, and 6 dominates the power spectrum at early times but the sum of $k=8$, 9, and 10 catches up with it at later times. The bottom frame in the figure compares the two sums without standard deviations to illustrate this competition.

In Fig. 8 the same three patterns shown in Fig. 5 are compared with their corresponding values of x versus s. In this case the originally flat interface would appear as a diagonal line in x versus s, and a finger causes the slope of x to decrease. Structure on a finger adds ripples to the region of low slope. In the figure one can easily see the importance at early times of the disturbances near the side walls. The side-wall disturbances gradually work their way to the center of the cell as can be seen for the two frames at later time. For each pattern in our ensemble, we have subtracted from x the ramp which would connect the initial and final values of x versus s and then constructed a power spectrum. The averages of these power spectra are shown in Fig. 9 for the same time values shown in Fig. 8. Early time flows are dominated by $k=1$, with the rest of the power also at low wave number. As time increases, power shifts to progressively higher wave-number. Figure 10 shows the sums of power in the two important regions to illustrate the time evolution of the system. The power sum of $k=1$, 2, and 3 increases at early times and later falls off. The power sum of $k=17$, 18, and 19 starts late and eventually begins to catch up. The latter sum includes the region predicted to have highest growth rate by the linear-stability analysis. The two sums are compared, without standard deviations, at the bottom of the figure. In both Figs. 7 and 10, the standard deviations do not change, whether one calculates them from the set of all individual points or by combining uncertainties of averaged powers for the individual wave numbers.

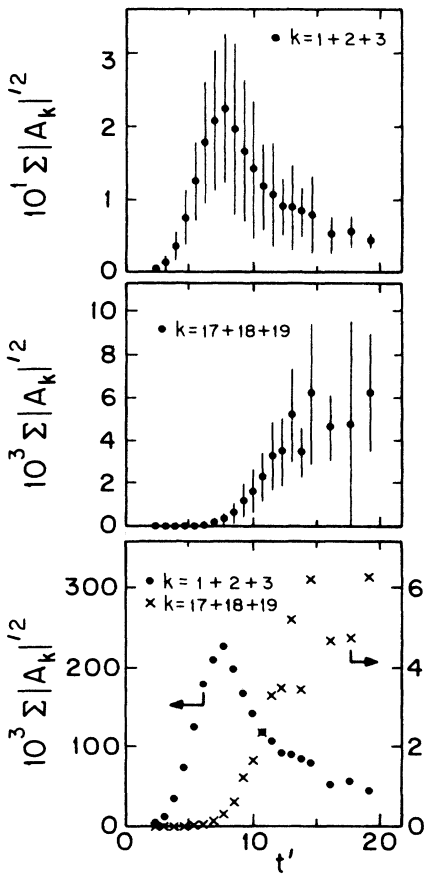

FIG. 10. Sums of the dimensionless power of the neighboring wave numbers vs dimensionless time for the x vs s representation of flow patterns.

IV. DISCUSSION

The various quantitative measures presented above for our Saffman-Taylor patterns suggest several important results of this investigation. These can be classified as relating to (a) the importance of fluctuations, (b) flow regularities in the linear regime, (c) characteristics of the transition to the nonlinear regime, and (d) flow regularities in the relatively early nonlinear regime.

A. Fluctuations

The standard deviations for the data shown in Figs. 1–10 indicate a significant amount of "noise" in the flow, but not such a great amount that the most important regularities are obscured. We obviously cannot comment on whether the noise level would continuously be reduced if we were to continuously improve the control of the experiment, but it has been demonstrated by several groups[16] that building in fluctuations by roughening the cell walls produces an enormously noisier situation. In our case, we measure the variation in the spectrophotometric-cell gap to be less than 2%. As was stated in Sec. II, by controlling the system temperature to 1 mK, we control the fluctuations in A and B to be less than 0.03% and 0.15%, respectively. The most strongly fluctuating quantities presented above are the contributions of individual wave numbers to the power spectra for x and y. This is to be expected, since the instability is, after all, broadband, and the surprising aspect is that the fluctuations are not larger. If the laboratory apparatus were as noisy as the algorithms for the computer simulations[8] which are used to model flows like this one, an ensemble of 14 realizations would be much too small to show such great regularity. It will be interesting to see whether plausible physical mechanisms can be added to the computer models to produce the greater stability seen in the laboratory patterns.

B. The linear regime

As was discussed above, in this paper we restrict ourselves to observations of regularities which do not depend on varying control parameters and which involve features which clearly stand out above the fluctuations. For the linear regime we can report two interesting observations.

First, the pattern we set up at relatively late stages in the linear regime is at least qualitatively in agreement with the fastest-growing wavelength expected from the linear-stability analysis. And second, the dominant disturbance which supplies the energy to set up the linear pattern comes from the side walls. Thus, even though the side-wall effects are less prominent here than in the many published cases with higher viscosity contrast,[3,9,10] we always observe the first fingers near the sides of the cell. These fingers, even though they have a width characteristic of the linear-dispersion relation, produce by their spacing the initial domination of the power spectra by low wave numbers. The x versus s curves clearly show the side-wall disturbances propagating into the interior at an average velocity $v \approx 0.4$ cm/sec $\approx 2U^*$, and thus presumably supplying the energy to drive the interior unstable much sooner than other available sources of noise would otherwise have done. Theoretical calculations and computer simulations normally impose periodic boundary conditions and thus cannot comment on the wall effects which are so important in virtually all experiments.

C. The transition from the linear regime to the nonlinear regime

The normal arbitrary definition of the time of this transition chooses that time at which the amplitude of the disturbance becomes equal to its wavelength. The situation is less obvious here because the amplitudes of the side-wall fingers reach their wavelength when the many central fingers are still quite small. If we ignore the amplitudes of the side-wall fingers, as we tacitly did in discussing the linear regime in Sec. IV B above, and use the amplitude of the central fingers to define the transition, we find that several of the features of the data discussed above show a dramatic break at the transition point. Thus the average curvature (Fig. 4) increases throughout the linear regime and is subsequently steadily reduced as long, relatively straight sections become more important features of the fingers. This break in the average curvature occurs at the same time that the power spectra for x and y (Figs. 7 and 10) cross over from being dominated by low wave numbers. In Fig. 10, the low-wave-number power actually declines after this time.

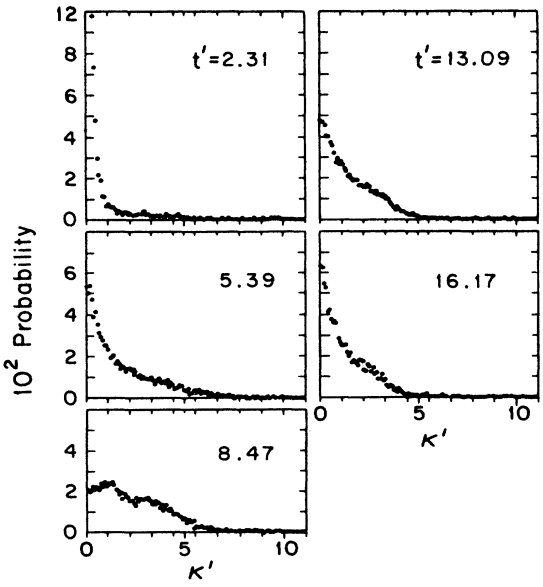

FIG. 11. Probability of occurence of a point of dimensionless curvature κ' along the interface vs κ'. These histograms are ensemble averages for the dimensionless times indicated. The bin size for κ' is 0.09.

The decrease in average curvature after this transition, appears not to be totally attributable to finger lengthening. This can be seen from Fig. 11, which shows histograms of occurrences of various values of the curvature along the interface at five times, including the same three times shown for all other quantities above (one time in the linear regime, one at the break point, and one well into the nonlinear regime.) While it is clear that lengthening fingers result in much higher probability for very low values of the curvature at late times it is also clear that the highest values of the curvature are seen at and before the transition point and do not appear at all in later stages of the flow.

D. The nonlinear regime

The most striking feature of the flow in the nonlinear regime is the lack of progress toward the steady-state single-finger solution. While this steady-state solution should not appear for the completely symmetric $A=0$ case, there is no reason to believe that it should not appear eventually for all nonzero values of A.[4-6] This experiment reaches values of dimensionless time at which larger-A systems have been seen to show dramatic progress toward the steady state, yet no sign of progress is seen in the present case, as can be seen from the time dependences of the power spectra shown above. In fact, one very notable feature as the system goes into the nonlinear regime is that the central fingers tend to catch up with the side-wall fingers and also tend to stay in line with each other. This tendency to stabilize fingers rather than have them compete is illustrated in Figs. 12 and 13, which show, respectively, the relative standard deviation in the length of fingers and the average length of the fingers as a function of time (as usual, the averages are taken over the entire ensemble). In each of these figures the upper plot shows an analysis which includes the side-wall fingers, while the lower shows an analysis which excludes one finger at each side of the cell.

While we cannot comment definitively on the question of whether or not our system would eventually go over to the single-finger pattern, we can make two interesting and relevant comments. First, we do not believe that the stabilizing of finger lengths can be attributed simply to the small aspect ratio [(length/width)=1] of our cell: to test this question we have recently constructed an annular Hele-Shaw cell by sealing the ends of two concentric cylinders: this cell has outer circumference 13 cm, gap 1 mm, and length 25 cm. Flow is initiated by inverting the axis of the cylinders (just as the flow in our smaller cell was initiated). It will take some time to extract quantitative detail from analysis of data from this cell, but we can

say already that the flow in the longer cell is qualitatively similar to that in the small cell over all flow stages which can be observed in the smaller cell. We cite this unfinished experiment here only because it is sufficient to show that our observations made with our small cell are not dominated by the nearness of the ends of the cell. It is only when the fingers approach within about 5 mm of the end walls of the smaller cell that one observes marked differences between the flows in the two cells. Second, the stabilizing of finger-length growth may well result from the fact that the cell is closed. Since the cell is closed, a mass-conservation constraint must be added to the normal Hele-Shaw requirements, and this may make a dramatic difference when a low-contrast A implies a weak driving force for the instability. Grier *et al.*[17] have suggested a stabilizing mechanism for electrodeposited tendrils which may carry over to the present case. They argue that the tendrils obey a one-dimensional Laplace equation rather than the two-dimensional equation which governs the supersaturated solution and that this difference can kill the Mullins-Sekerka instability if the driving force is weak. Carried over to the present case the argument would say that, when A is small, a longer neighboring finger does not shield a finger very much from the driving gradient, while mass already in the finger cannot communicate effectively with mass in other fingers. In such a scenario all fingers can plausibly keep growing and being fed from the end reservoir. Such an assumption is consistent with the results of the closed cell

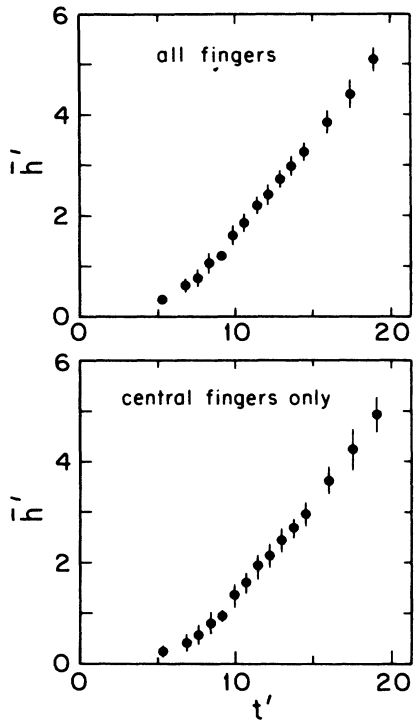

FIG. 13. Ensemble average of the average dimensionless finger length vs dimensionless time. The top plot shows the result including all fingers and the lower plot shows the result excluding the fingers nearest the side walls.

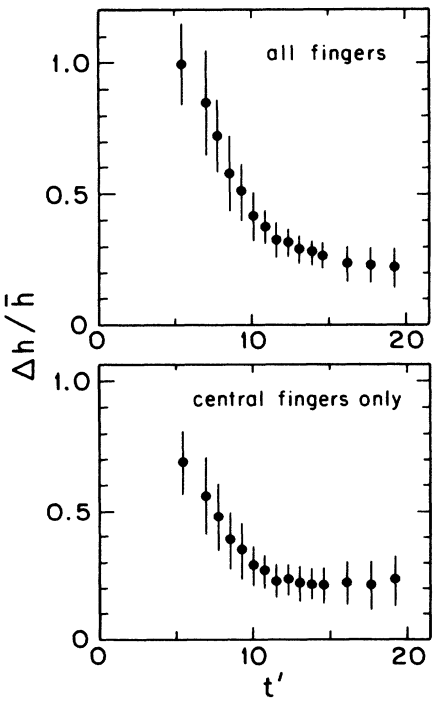

FIG. 12. Relative standard deviation of the finger length vs dimensionless time. The top plot shows the result when all fingers are included while the lower one shows the result when the fingers along the side walls are excluded.

calculations of TA (Ref. 7) and with our observations, but it would be very interesting to understand in detail the extra physics needed to stabilize the fingers and to know whether or not an extremely long closed cell would eventually go over to a single-finger steady state. We know from Maxworthy's work[10] and from closed cells which we have constructed for high-A flows (air and oil) that the fingers do not stabilize when A is large; i.e., noticeable progress is made toward the single-finger steady state in a closed cell of small aspect ratio if $A \approx 1$.

A final feature of low-A flow in the nonlinear regime is worth noting. Essentially all fingers tend to show "ballooning" finger tips, as was mentioned above. These balloons form long before the fingers come near the ends of the cell, and they are also seen at a similarly early stage of the flow in our annular cell. Thus their appearance cannot be a simple artifact of having a cell of low aspect ratio, although they may well arise from having a closed cell. These balloons also appear in the TA calculations when A is small. We do not understand the mechanism for the formation of these balloons, but they begin to form just at the onset of the nonlinear regime and thus coincide with the disappearance of points of very high curvature (as seen in Fig. 11). While it is tempting to ascribe this tendency to an annealing of high curvature (and thus high Gibbs-Thompson pressure drop across the interface), we cannot confidently make such a claim, since we cannot observe the presumably much higher contributions to the total curvature which occur in the narrow-gap direction. As was mentioned above and in Ref. 15,

the curvature we report codes all local information in the two-dimensional pattern but does not bear any necessary relation to the total curvature needed to calculate the Gibbs-Thompson pressure drop.

V. SUMMARY AND CONCLUSIONS

We have measured 14 realizations of low-A Saffman-Taylor flow under as close to identical flow conditions as our apparatus would permit. We observe $\approx 20\%$ fluctuations in the crudest quantitative measures of the interfacial patterns (Figs. 2–4), whereas the control-parameter fluctuations are measured to be only $\Delta A/A \lesssim 0.0003$ and $\Delta B/B \lesssim 0.0015$, respectively. Fourier transforms of the x versus s and y versus s patterns shown in Figs. 6 and 9 show significantly larger fluctuations for individual wave numbers, but this is not surprising since the instability is broadband. The disturbance which initiates the pattern evolution clearly comes from the side walls and can be observed to propagate toward the center of the cell while the pattern is still within the linear regime (Fig. 8). Without side-wall perturbation it would presumably take other sources of random noise significantly longer to exploit the instability. As the interface enters the nonlinear regime, several of the quantitative pattern measures show a rather abrupt change (Figs. 4, 7, 10, and 11). In the nonlinear regime no progress is seen toward the presumed single-finger steady-state solution. (Large-A flows show dramatic progress toward the steady state at even earlier dimensionless times and even in closed cells of small aspect ratio.) Thus the low-A flows may not have the same (or any) steady state; rather than the fingers competing with one another, the finger lengths seem to evolve toward a narrower distribution of lengths in the nonlinear regime (Figs. 12 and 13).

ACKNOWLEDGMENTS

We would like to thank David Jasnow, Subir Sarkar,and Steven N. Rauseo for helpful discussions. This work was supported by the U. S. Department of Energy under Grant No. DE-FG02-84ER45131.

[1]P. G. Saffman and G. I. Taylor, Proc. R. Soc. London, Ser. A **245**, 312 (1958).

[2]S. Hill, Chem. Eng. Sci. **1**, 247 (1952); R. L. Chuoke, P. van Meurs, and C. van der Poel, J. Petrol. Tech. **11**, 64 (1959).

[3]C. W. Park and G. M. Homsy, J. Fluid Mech. **139**, 291 (1984).

[4]J. W. McLean and P. G. Saffman, J. Fluid Mech. **102**, 455 (1981); J. M. Vanden-Broeck, Phys. Fluids **26**, 2033 (1983); D. Kessler, J. Koplik, and H. Levine, Phys. Rev. A **30**, 3161 (1984); D. A. Kessler and H. Levine, *ibid.* **32**, 1930 (1985); **33**, 2621 (1986); **33**, 2634 (1986); D. Bensimon, *ibid.* **33**, 1302 (1986); S. Sarkar and D. Jasnow, *ibid.* **35**, 4900 (1987); A. T. Dorsey and O. Martin, *ibid.* **35**, 3989 (1987); B. I. Shraiman, Phys. Rev. Lett. **56**, 2028 (1986); D. C. Hong and J. S. Langer, *ibid.* **56** 2032 (1986); R. Combescot, T. Dombre, V. Hakim, Y. Pomeau, and A. Pumir, *ibid.* **56**, 2036 (1986); A. J. DeGregoria and L. W. Schwartz, J. Fluid Mech. **164**, 383 (1986).

[5]D. Bensimon, L. P. Kadanoff, S. Liang, B. I. Shraiman, and C. Tang, Rev. Mod. Phys. **58**, 977 (1986).

[6]P. Tabeling and A. Libchaber, Phys. Rev. A **33**, 794 (1986); P. Tabeling, G. Zocchi, and A. Libchaber, J. Fluid Mech. **177**, 67 (1987).

[7]G. Tryggvason and H. Aref. J. Fluid Mech. **136**, 1 (1983); **154**, 287 (1986).

[8]S. Liang, Phys. Rev. A **33**, 2663 (1986); T. Vicsek, Phys. Rev. Lett. **53**, 2281 (1984); P. Meakin, F. Family, and T. Vicsek, J. Colloid Interface Sci. **117**, 394 (1987); J. Nittman, G. Daccord, and H. E. Stanley, Nature **314**, 141 (1985).

[9]J. V. Maher, Phys. Rev. Lett. **54**, 1498 (1985); in *The Physics of Finely Divided Matter,* edited by N. Boccara and M. Daoud (Springer-Verlag, Berlin, 1985), pp. 252–257.

[10]T. Maxworthy, J. Fluid Mech. **177**, 207 (1987).

[11]S. C. Greer, Phys. Rev. A **14**, 1770 (1976).

[12]Hellma Cells Inc., Forest Hills, NY.

[13]Methyl Red, Fisher Scientific Company, Fair Lawn, NJ.

[14]GTCo Corporation, Rockville, MD.

[15]S. N. Rauseo, P. D. Barnes, Jr., and J. V. Maher, Phys. Rev. A **35**, 1245 (1987).

[16]J.-D. Chen and D. Wilkinson, Phys. Rev. Lett. **55**, 1892 (1985); E. Ben-Jacob, R. Godbey, N. D. Goldenfeld, J. Koplik, H. Levine, T. Mueller, and L. M. Sander, Phys. Rev. Lett. **55**, 1315 (1985).

[17]D. G. Grier, D. A. Kessler, and L. M. Sander, Phys. Rev. Lett. **59**, 2315 (1987).